I. J. Transport Phenomena, Vol. 1, pp. 51–65
Reprints available directly from the publisher
Photocopying permitted by license only

Transient Phenomena and Non-equilibrium in Two-phase Flow with Phase Change

F. MAYINGER

Lehrstuhl A für Thermodynamik, Technische Universität München, 85747 Garching, Germany

(Received 25 June 1997)

Non-equilibria in two-phase flow can be observed not only under transient conditions, like blow-down, but also in steady-state flow, if high heat fluxes are applied to the boiling liquid. Steady-state nucleate subcooled boiling is locally a highly transient process. Within a few milliseconds, bubble formation and bubble collapse occur with highly complicated transport phenomena. The superheated boundary layer near the wall not only shows a very dynamic behavior, but also undergoes a state of high thermodynamic non-equilibrium. Strong non-equilibrium effects can also be observed, with post-dryout heat transfer in dispersed flow. Transient flow occurs during depressurization procedures. In this case, the two-phase mixture reaches neither thermodynamic nor fluid-dynamic equilibrium. Depressurization phenomena in binary or ternary are of special interest if the components have a very different volatility. Flashing delay in those mixtures can be very different from that in pure substances. Examples for non-equilibria situations are presented for two-phase flow conditions, like during subcooled boiling, spray cooling after dryout, and during blow-down.

Keywords: Subcooled boiling, blow-down, flashing, post-dryout, spray cooling, optical measuring techniques

1. INTRODUCTION

Non-equilibrium in two-phase flow can be of thermodynamic, thermal and fluid-dynamic nature. To distinguish between thermodynamic and thermal non-equilibrium is not always easy. Thermodynamic disequilibrium, for example, exists in superheated liquid during boiling delay and in a subcooled vapor before condensation starts. Such situations can originate from fast transients, for example, during rapid depressurization of a slightly subcooled liquid or a superheated vapor.

Thermal non-equilibrium is assorted to non-adiabatic flow with high heat flux densities. An example for a situation with thermal non-equilibrium is post-dryout spray cooling, when small liquid droplets, having saturation temperature, are embedded into superheated vapor, where locally large temperature gradients may additionally exist in the vapor.

In this paper, non-equilibrium observations will be mainly limited to thermodynamic and thermal non-equilibrium. Such situations occur in any once-through evaporator, in which subcooled liquid

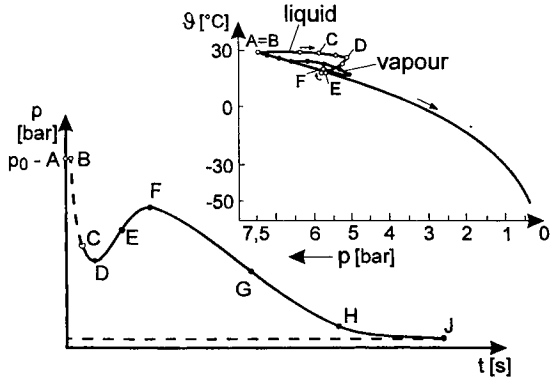

FIGURE 1 Thermodynamic non-equilibrium at the pressure relief of vapor–liquid mixtures.

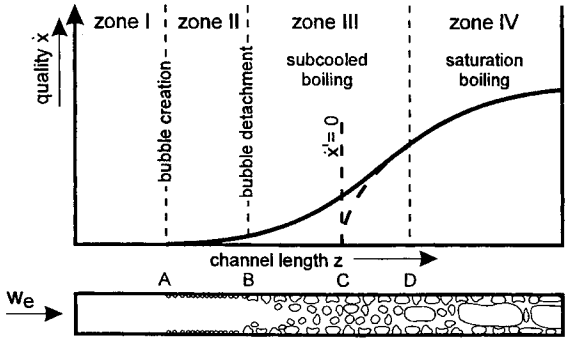

FIGURE 2 Boiling regions with subcooled inlet at a high heat flux; $\dot{x}$: real quality, x: quality at the thermodynamic equilibrium.

enters and superheated vapor gushes out. In transient, temporally non-steady situations, thermodynamic, thermal, and fluid-dynamic non-equilibria may be overlapped. The thermodynamic non-equilibria in a fluid (refrigerant R12) during a depressurization are briefly shown in Fig. 1. The refrigerant (Viecenz, 1980) was rapidly depressurized and immediately after starting (B) the depressurization, a rapid pressure decrease, but almost no temperature change in the liquid was monitored, while the temperature in the vapor followed the saturation curve. The liquid showed strong boiling delay. At the moment C, flashing starts in the liquid, which finally (D to F) becomes so large that the production of volume, due to evaporation, is larger than the volumetric out flow through the nozzle. During this period, the thermodynamic non-equilibrium in the liquid is reduced due to the non-equilibrium between volumetric out flow and vapor production, the pressure can recover until the moment F. From there on, the thermodynamic conditions in the vessel follow the saturation line.

2. SUBCOOLED BOILING

With high heat fluxes from the wall, there exists a considerable temperature gradient in the boundary layer with a peak temperature at the wall, well above the saturation temperature of the liquid in the channel. This results in a nucleation and bubble formation in the superheated zone of the boundary layer. As soon as a bubble has grown to a diameter larger than the thickness of the boundary layer, or as soon as the bubble is detaching from the wall and traveling out of the boundary layer, it starts to condense again, because it reaches the subcooled bulk. The void fraction in this part of the evaporating channel is a result of the balance between bubble formation and bubble condensation.

As shown in Fig. 2, four regimes of heat transport and fluid flow are distinguished in the literature. In zone I, only single-phase liquid flows through the channel. With increasing liquid temperature also the wall temperature rises, if there exists constant heat flux along the channel. Finally the wall temperature is high enough to activate the first nuclei, but the tiny bubbles, originating from the nucleation, condense again immediately at the wall without departing, due to the thin boundary layer (zone II). On its way through the channel, the difference between saturation temperature and bulk temperature in the liquid becomes smaller, the condensation process is reduced in its intensity, and so bubbles can depart from the wall and travel downstream (zone III). At the elevation, where thermal equilibrium would predict just saturation conditions ($\dot{x} = 0$), already considerable void fraction exists. Finally thermal equilibrium is reached in

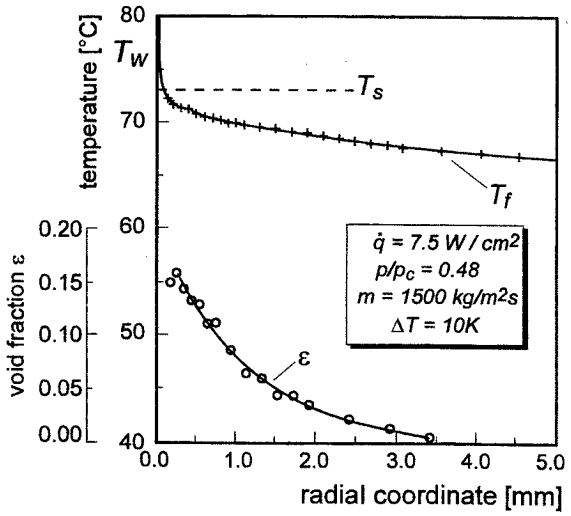

FIGURE 3 Radial temperature- and void distribution with subcooled boiling.

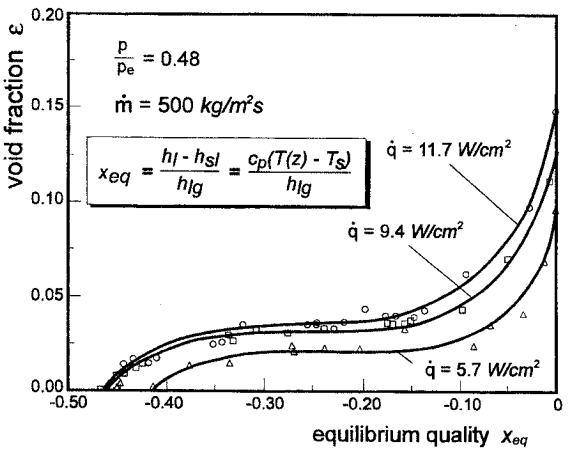

FIGURE 4 Axial void distribution (in terms of quality) with subcooled boiling.

the channel which means that all heat, added to the fluid, is converted into vapor production.

However, there is also another phenomenon affecting local void fraction, namely, the slip between the phases. The velocity profile in connection with the vapor distribution influences the void fraction, because with high velocity, the same amount of fluid can be transported in a narrower area than with low velocity. Figure 3 presents the distribution of fluid temperature T_f and void fraction ε across an annular channel, where the inner wall was heated. The fluid was the refrigerant R12. In spite of the fact that most of the fluid had a temperature well below the saturation temperature T_s, there was a considerable amount of void in the channel near the heated wall. This two-phase layer had a thickness of less than 4 mm with a maximum of 15 percent void in the immediate vicinity of the heated wall (Bräuer *et al.*, 1990, see Fig. 3).

Measuring the void fraction along the length of the annular channel for various heat flux densities, one gets a void distribution as demonstrated in Fig. 4 (Bräuer *et al.*, 1990). In this figure, the abscissa does not represent the length and, by this, the traveling path of the fluid through the channel directly, but the equilibrium quality of the fluid is plotted there, which is calculated from the heat input by assuming thermodynamic and thermal equilibrium. This calculation predicts negative quality, subcooled liquid, for almost the full length of the channel. The channel was uniformly heated and therefore this equilibrium quality only differs by a constant factor — depending on the heat flux and the area of the heated surface — from the length coordinate of the channel.

After very first nucleation, which starts at high subcooling in the example, shown in Fig. 4, void fraction starts to grow rapidly. After a short distance from this onset of nucleation, the gradient of the void fraction becomes much smaller, until it is increasing again when approaching saturation conditions. Reasons for these variations in the gradient of the void fraction are competitive effects between bubble growth and bubble condensation, as well as slip conditions between the phases. For better understanding of the phenomenon, we have to look for bubble dynamics at the wall under these non-equilibrium conditions. The phenomena are highly transient and, therefore, we need an inertialess method which, in addition, must be non-invasive to avoid disturbing of the flow and of the nucleation. Such a method is, for example, the holographic interferometry, together with high-speed cinematography, a detailed description of

which is given in Mayinger and Panknin (1974) and Mayinger (1994).

An example of holographic interferograms of boundary conditions with subcooled boiling near a heated wall is illustrated in Fig. 5. The black lines — called *interference fringes* — have to be interpreted in such a way that each black line represents an isotherm and the temperature difference between each of two neighboring lines is constant at any position in the interferogram. This means that there is a steep temperature gradient, if two interference fringes are near together, and there is a flat temperature plateau, if they are far apart.

The example in Fig. 5 shows a simple flow boiling process, where subcooled water was slowly flowing over a horizontal electrically heated surface. Due to the heating, nucleation started in the superheated boundary layer and bubbles were forming.

Boiling on a heated surface is a statistical process and nucleation, as well as recondensation of a forming bubble, cannot at all be described by a simple theory. This is demonstrated in Fig. 5 as well. The sequence of interferograms, presented there, covers a total timespan of approximately 5 ms.

In the middle of the first interferogram, near the heated wall, we observe a relatively thick boundary layer with flat temperature distribution. There a bubble starts to grow (scene 0.3 ms), grows and recondenses again, after reaching the subcooled bulk of the fluid. Growth and recondensation of this bubble is finished after 4.7 ms.

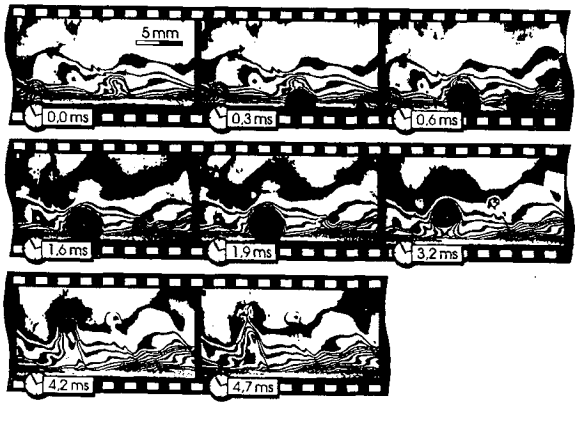

FIGURE 5 Detachment and recondensation of bubbles under various boundary conditions.

Another bubble, also at the moment 0.3 ms, starts to grow under a position of a boundary layer with high temperature gradient. Due to the high temperature gradient, this bubble grows explosively within 0.3 ms, moves very fast into the subcooled bulk, and condenses there as rapidly as it was grown. Its total lifespan is less than half that of the first bubble. So bubble growth and bubble recondensation are strongly dependent on the boundary layer conditions.

For a theoretical description of bubble growth and bubble condensation, we would need a very sophisticated information about the temporarily and locally very fast changing situations of non-equilibria in the boundary layer. With our present mathematical tools and our limited knowledge about turbulence — especially in two-phase flow — a reliable and precise description of the boundary layer is not possible, according to my opinion. The situation becomes even more difficult if we would like to describe the phase-interface phenomena at the surface of the bubble when it recondenses. But, for measuring these phenomena with holographic interferometry, we need a more sophisticated optical arrangement. With very high heat-transfer coefficients, the boundary layer at the heat-transferring surface becomes very thin, down to a few hundreds of a millimeter. In this case, we use a method, called *finite-fringe-method*, where we produce a pattern of parallel interference fringes artificially, which at first has nothing to do with the temperature field (Nordmann and Mayinger, 1981). The direction of the pattern can be selected as one likes. By imposing a temperature field, due to the heat-transport process, this pattern of the parallel interference fringes is then distorted. The distortion or deflection of each fringe from its original parallel direction is a measure of the temperature gradient at this spot and allows to deduce the heat flux and by this, the heat-transfer coefficient.

In Fig. 6, this method is applied for monitoring the boundary layer and, by this, also the heat

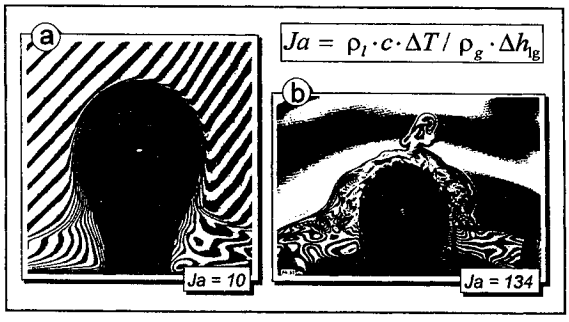

FIGURE 6 Phase interface boundary layers with heat-transfer and inertia-controlled condensation.

transfer at the phase-interface at a bubble, filled with saturated vapor and condensing in an isothermal subcooled liquid of the same substance (Nordmann and Mayinger, 1981). The velocity of the condensation and, by this, the movement of the phase-interface can be controlled either by the heat-transfer process, or — at very high subcooling — by inertia forces. The left interferogram in Fig. 6 demonstrates the situation when the heat transfer dominates and the right one gives an impression of inertia-controlled condensation. In the latter case, the heat-transfer coefficient cannot be measured by holographic interferometry, because there is no laminar boundary layer at the phase-interface.

The quantitative evaluation of these finite-fringe interferograms, shown in Fig. 6 and, by this, the transformation of the interference pattern into local heat-transfer coefficients is a very complicated process, which cannot be explained here. Reference is made to the literature, for example, Mayinger and Panknin (1974), Nordmann and Mayinger (1981), Mayinger (1994), and Chen *et al.* (1991).

A sequence of evaluations of such interferograms is presented in Fig. 7. Saturated steam is blown through a capillary into slightly subcooled water. A bubble is formed at the outlet of the capillary and the condensation process starts immediately. For a short period (No. 2 in Fig. 7), the condensation at the phase-interface reduces the volume of the bubble to such a large extent that there cannot be enough steam fed into the bubble via the flow through the capillary. Therefore, during the period

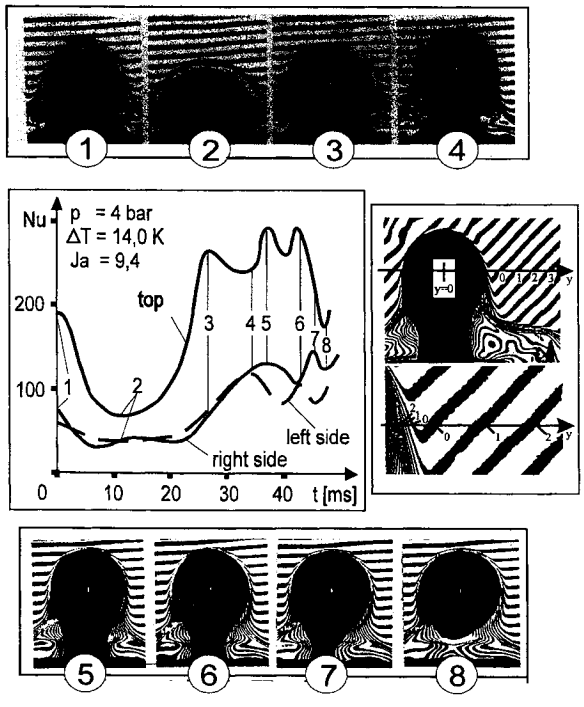

FIGURE 7 Heat transfer at the phase-interface of a condensing steam bubble.

"2", the bubble takes a "squatting position", which increases the thickness of the boundary layer at the top of the bubble. This again results in a strong decreasing of the heat-transfer coefficient there, because the boundary layer consists of saturated liquid. Now the steam flowing from the capillary can overcome the condensation rate and the bubble is again growing. This goes together with an increasing of the heat-transfer coefficient. Finally, the bubble separates from the nozzle and leaves the area where the holographic interferometry could watch the phenomena. The heat-transfer coefficient is strongly oscillating during the condensation period and it is much smaller at the side of the bubble than at its top. The reason for the latter phenomenon is that the boundary layer, starting to be formed at the top, becomes thicker via the equator, when the bubble is growing and, by this, moving upward into the subcooled bulk.

It looks very complicated to describe the local and temporal variations of the heat-transfer coefficient

with a correlation. However, the situation becomes much simpler, if one is only interested in the average heat-transfer coefficient — averaged versus time and circumference of the bubble. Data for the average heat-transfer coefficient with condensing bubbles are shown in Fig. 8 under conditions, when the bubble is still adhering to the wall (Chen, 1985). In this figure, the Nusselt number is plotted versus a dimensionless subcooling, expressed in the terms of the Jacob number

$$Ja = \frac{\rho_l \cdot c_l \Delta T_{sub}}{p\nu \cdot \Delta h_{lg}}. \quad (1)$$

After the bubble left the wall and is moving upward, the heat-transfer situation at the phase-interface changes, due to the larger relative velocity between subcooled liquid and steam. In this case, the averaged heat-transfer coefficient can be described by the simple equation

$$Nu = 0.6 Re^{0.6} Pr^{0.5}. \quad (2)$$

In both cases, fixed and moving bubble, the Reynolds number is formed with the diameter of the bubble at the moment of departure, the relative velocity between bubble and liquid, and the viscosity of the liquid. The transport properties in the Prandtl number are referred to the liquid. At high Jacob numbers — above 70 — inertia-controlled phenomena start to dominate and then the optical measuring method starts to fail, as shown in Fig. 8, and also the heat-transfer equations are no longer valid.

Modern optical measuring techniques can give good insight into the non-equilibrium situations of an apparently simple heat-transfer process, like subcooled boiling. However, we are still far away from understanding the thermo- and fluid-dynamic phenomena completely, involved in this process. To formulate mathematical models, describing these thermo- and fluid-dynamic situations, seems to be even further out of our present horizon.

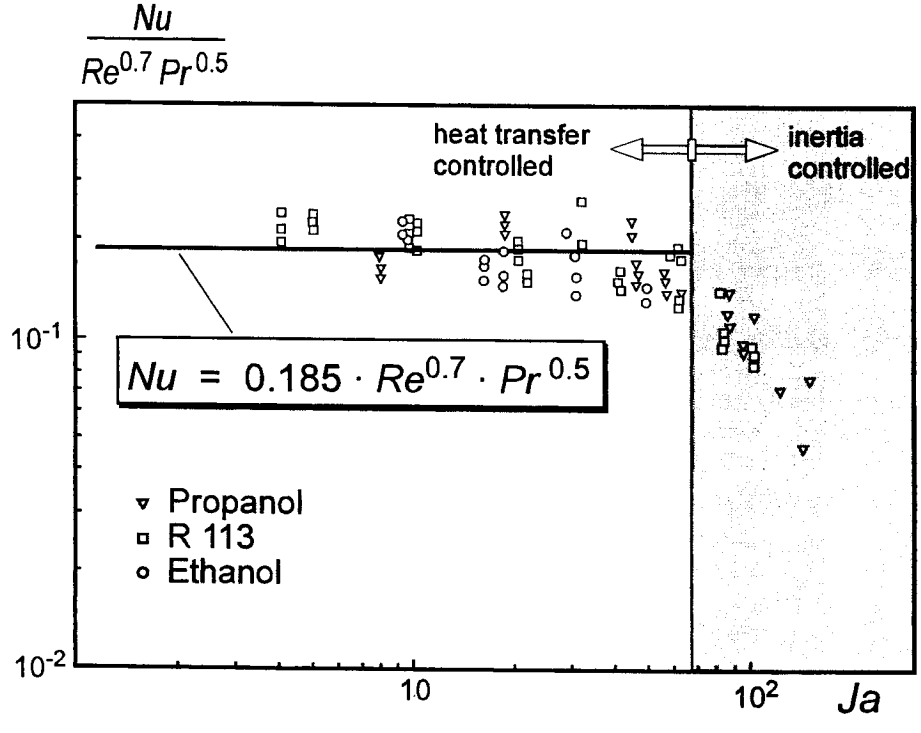

FIGURE 8 Heat transfer at the phase-interface of a condensing bubble.

3. POST-DRYOUT HEAT TRANSFER

Dispersed flow film boiling is of great importance in many industrial applications, for example, in the design and operation of once-through steam generators, in the analysis of a hypothetical loss-of-coolant accident of a nuclear reactor and in the evaluation of various metallurgical and cryogenic processes. The heat-transfer mechanism of dispersed flow has been well investigated in the literature, however, mostly for simple geometries, like straight tubes.

The fluid-dynamic situation becomes much more complicated if the dispersed flow travels through a bend instead of a straight tube. In addition to momentum and gravity forces, centrifugal forces are acting on the fluid, resulting in the effect that the more dense phase — the liquid — is moving to the outer perimeter of the bend. These centrifugal forces are creating pressure forces, acting into the opposite direction. From these pressure forces, a secondary flow can originate, resulting in a very complicated flow pattern of a helical nature, as sketched in Fig. 9.

With dispersed flow, these forces not only influence the distribution of the droplets versus the cross-section of the channel, but they also have a strong influence on the temperature distribution of the continuous phase — the vapor — in the channel. To better understand the phenomena with dispersed flows in bends, experiments were carried out by Mayinger and Wang (1994) and by Lautenschlager *et al.* (1994), using the refrigerant R12 as fluid. Dispersed flow was produced through the dryout of an annular flow in the vertical part of the Joule-heated test-section. The dryout point was regulated to occur at a position 2.5 m, before the bend inlet, to allow a sufficient length of dispersed flow development. So the test-section consists of a vertical part and a 90° bend.

Immediately in front of the bend, an axissymmetric temperature distribution was observed, as shown in Fig. 10. This profile changes considerably along the flow in the bend. Behind the bend, the temperature of the superheated vapor is much higher at the inner side, due to low droplet concentration there. The droplets that were migrating to the outer side are improving the cooling capability there, which results in a slight decrease of the vapor temperature in the outer boundary layer (see Fig. 10).

Due to the thermal non-equilibrium between superheated vapor and saturated droplets, there is heat transfer between the phases, resulting in an evaporation of the liquid, which reduces the temperature of the vapor. Lower vapor temperature, in connection with higher droplet concentration, produces a better heat transfer from the wall to the fluid and, therefore, the wall temperatures diverge along the bend (Lautenschlager *et al.*, 1994).

It is now of interest to get information about the change of the distribution of the droplets in the fluid

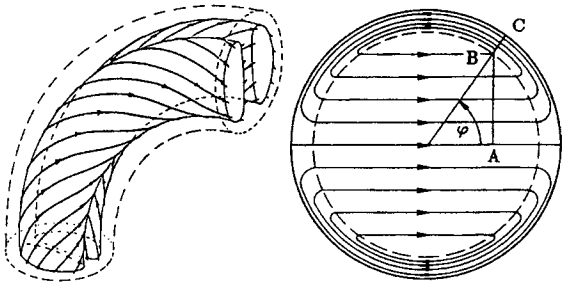

FIGURE 9 Secondary flow in a bend.

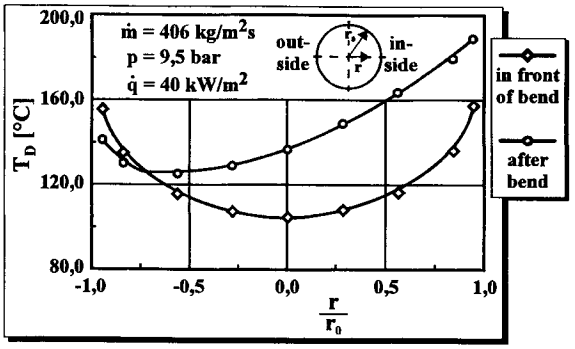

FIGURE 10 Temperature profile of the vapor before and after a 90° bend.

on their way through the bend. An impedance probe was used to measure the local liquid fraction in different regions of the cross-section (Mayinger and Wang, 1994; Lautenschlager *et al.*, 1994; Klug and Mayinger, 1992; 1994; Wang, 1993). A remarkable change of the bulk flow structure and of the droplet dynamics was observed due to the centrifugal forces and also due to the secondary flow, produced by the bend. Figure 11 shows the change in the phase distribution along the path of the flow through the bend for a total mass flow rate of 1240 kg/m^2. The experiments showed that phase separation, due to the centrifugal effect, appears immediately after the bend inlet. The liquid fraction increases significantly from 0° to 15° in the outer side region, whereas it decreases correspondingly in the inner side region. Dispersing continues until 45° bend angle, where the effect of the secondary flow reversal becomes noticeable. Figure 11 shows that a large amount of liquid appears in the inner region again at the end of the bend, that is, near the bend outlet. This fact of liquid distribution can be explained by a liquid film or a dense droplet cloud inverting along the wall.

As mentioned, centrifugal forces — like gravity forces — produce a pressure force, acting in the opposite direction. The droplets in the bulk of the flow are mainly affected by the centrifugal force and they therefore are moving outward. On the other side, particles in the boundary layer near the wall, where friction has a considerable influence, may follow the pressure force and, by this, they are slowly moving inward.

This change in the phase distribution can have a significant influence on the heat-transfer coefficient along the wall of the bend. Especially under intermediate and large mass fluxes, together with low heat fluxes, this migration of the droplets, and also that of the liquid particles in the boundary layer near the wall, may result in a rewetting of the wall.

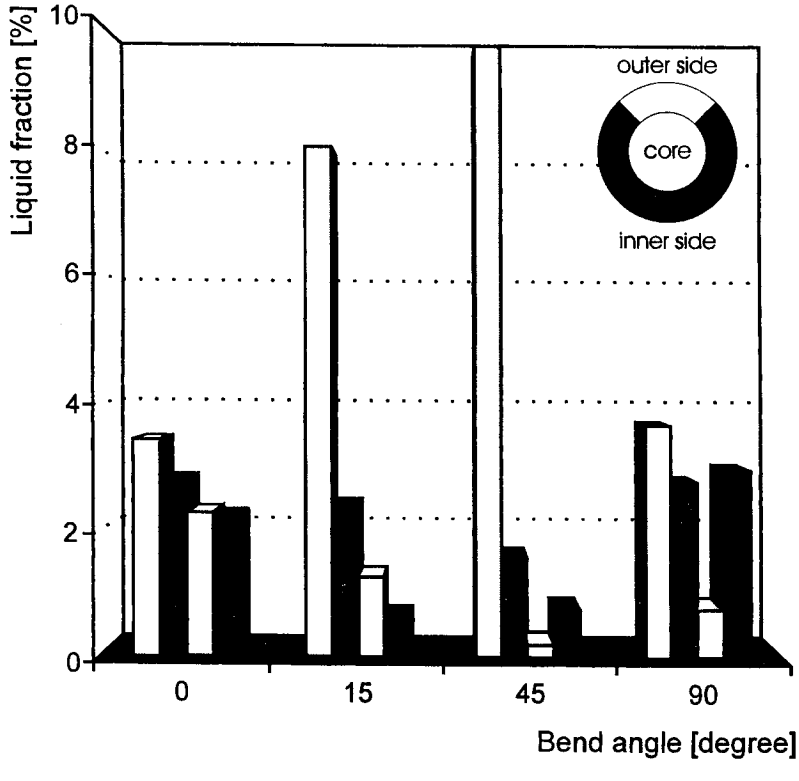

FIGURE 11 Liquid fraction at various positions of a bend.

Due to a massive droplet impingement, the outer wall may be quickly quenched to a value near the saturation temperature, resulting in an order-of-magnitude increase of the heat-transfer coefficient, as can be seen from Fig. 12. Under low wall superheat, droplets maintain stable contact on the outer wall, where they can easily link together to form a continuous liquid film. This has been confirmed from liquid fraction measurements, shown in Fig. 11.

Further downstream, because of the action of the secondary flow and the gravity, rewetting is propagated from the outer side to the inner side, where small wall superheat and high liquid fraction are observed. Also there, the local heat-transfer coefficient is consequently greatly enhanced. In Fig. 12 data are also presented which were calculated assuming single-phase vapor flow at the wall. For information on how this calculation was performed and also about details of the measuring technique, reference is made to Wang (1993).

4. HIGHLY TRANSIENT FLOW

Highly transient flow is readily observed during depressurization procedures by opening a valve or unwittingly due to a crack in a pipe. In the literature, one can find several publications on critical mass flow (Moody, 1965; Henry and Fauske, 1971; Sozzi and Sutherland, 1975) and on phase separation in the pressure vessel, which is undergoing the depressurization (Mersmann, 1977; Sterman, 1965). Most experiments on these subjects were done with water as fluid. Very little is known about the phenomena — thermodynamic non-equilibrium and flashing — in the pipe, which is linking the pressure vessel with the crack or the opening valve. Briefly a few experiences will be presented here, which were gained from a simple experimental set-up, shown in Fig. 13. This experimental facility consists of three main components, a pressure vessel containing the fluid, a depressurlization pipe, through which the flashing fluid flows,

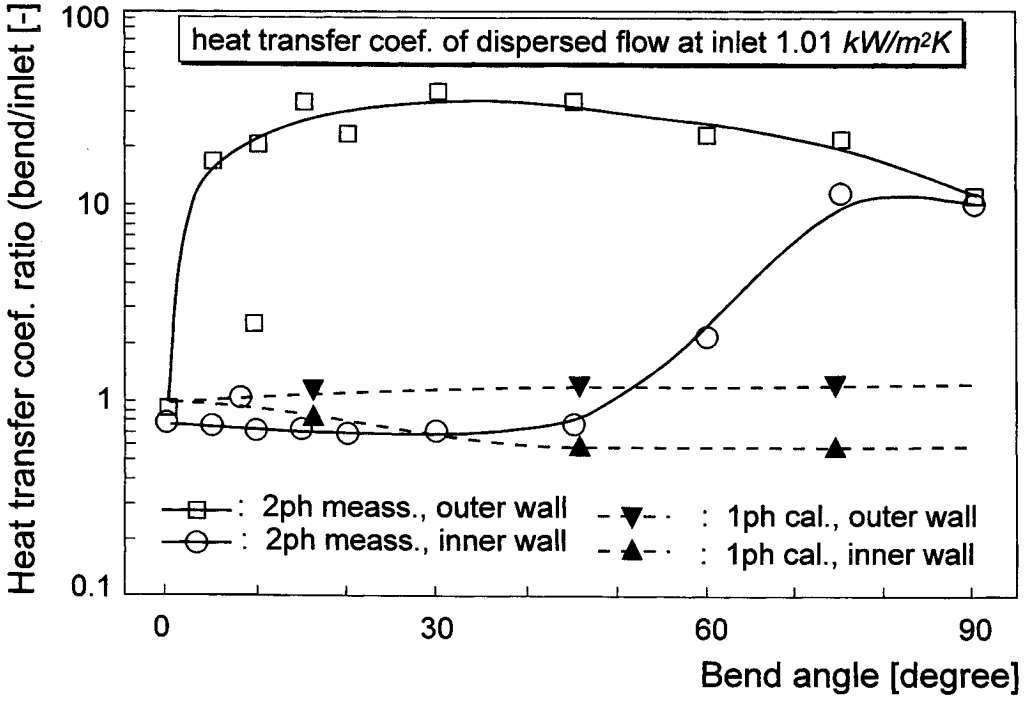

FIGURE 12 Heat transfer of dispersed flow versus a bend.

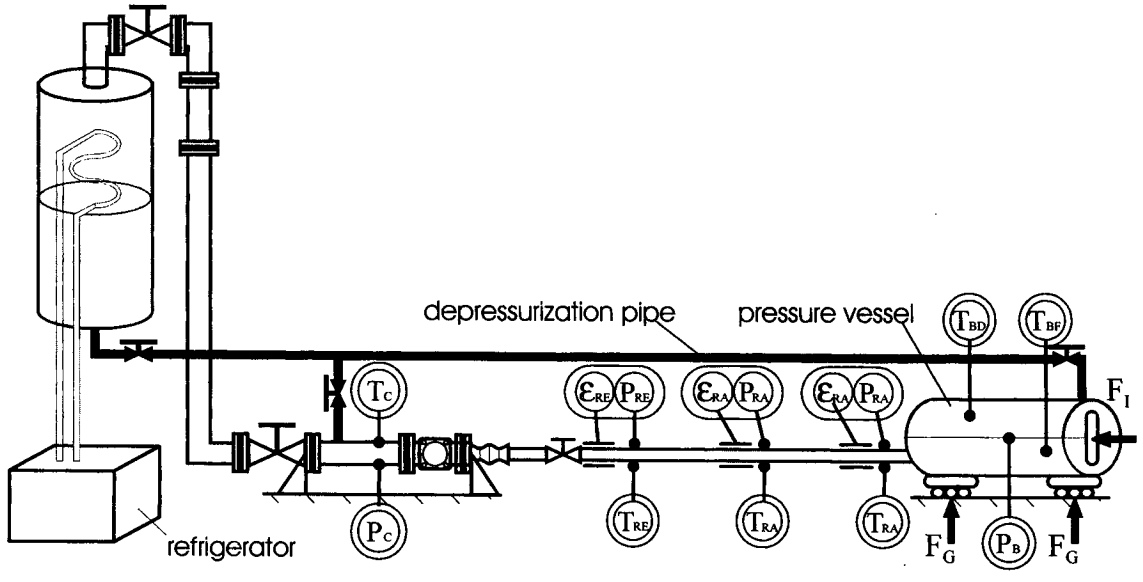

FIGURE 13 Experimental set-up for blow-down studies.

and a low-pressure containment, in which the depressurized two-phase mixture is captured. The high-pressure part and the low-pressure system of the facility are separated by a burst disc, mounted at the end of the pipe. Three different pipe lengths were used, having L/D ratios of 70, 170, and 240, respectively. The pipe had a diameter of 10 mm and orifices of 3 or 5 mm could be fixed at its downstream end. Experiments without an orifice were also performed (see Fig. 13).

Vessel and depressurization pipe were mounted on a movable carriage, so that the momentum of the flashing flow, leaving the pipe through the orifice, could be measured via a force gauge against which the pressure vessel was pushing. Four other dynamometers support the pressure vessel from below, indicating the instantaneous mass inventory of the fluid in the vessel. So the mass flow rate out of the vessel could be measured at any moment during the blow-down. The local and temporal value of the void fraction in the pipe, during the depressurization was measured by a special impedance sensor, acting on a capacitive basis and using the difference in the dielectric constant of vapor and liquid. For details of the experimental set-up, reference is made to Mayinger *et al.* (1995). These impedance sensors were placed on three positions of the long pipe ($L/D = 240$), as indicated in Fig. 13. The other pipes had only two ($L/D = 170$) and one sensor ($L/D = 70$), respectively. The electrodes of this sensor were installed in the pipe-wall in such a way that they were non-intrusive to the two-phase flow. At each position of an impedance sensor, also the fluid temperature and the local pressure were measured. Further thermocouples and pressure sensors were arranged in the pressure vessel. The arrangement of the thermocouples in the pressure vessel is shown in Fig. 14.

Experiments were performed with propane, with butane, and also with a mixture of 50 mole percent propane and butane. Before initiating the depressurization, the fluid in the vessel and in the pipe was kept in saturation conditions by an electrical heating system, attached to the outer walls. The pressure vessel had a capacity of 30 l. In the experiments, it was filled with a fluid mass between 5 and 10 kg.

Figure 15 presents the thermodynamic non-equilibrium in the pressure vessel during a blow-down through a pipe of $L/D = 170$, with butane as fluid, throttled at the outlet by an orifice of 5 mm. In the upper diagram of Fig. 15, the temporal course

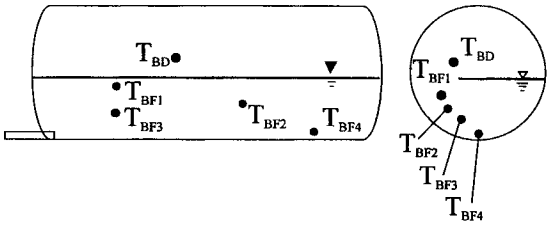

FIGURE 14 Positions of thermocouples in vessels.

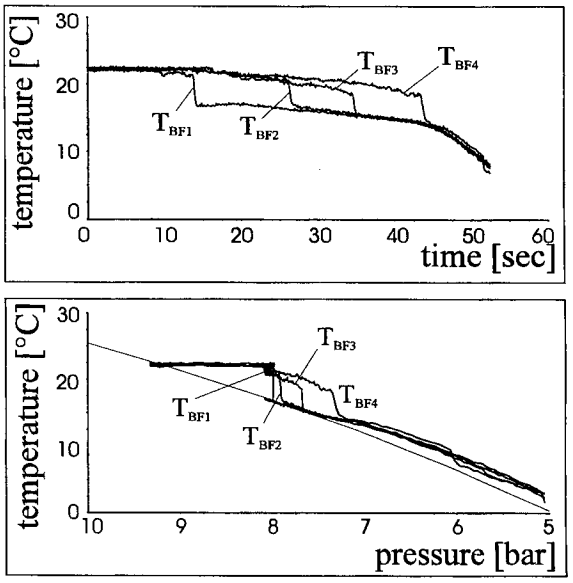

FIGURE 15 Thermal non-equilibrium in the vessel during blow-down (propane).

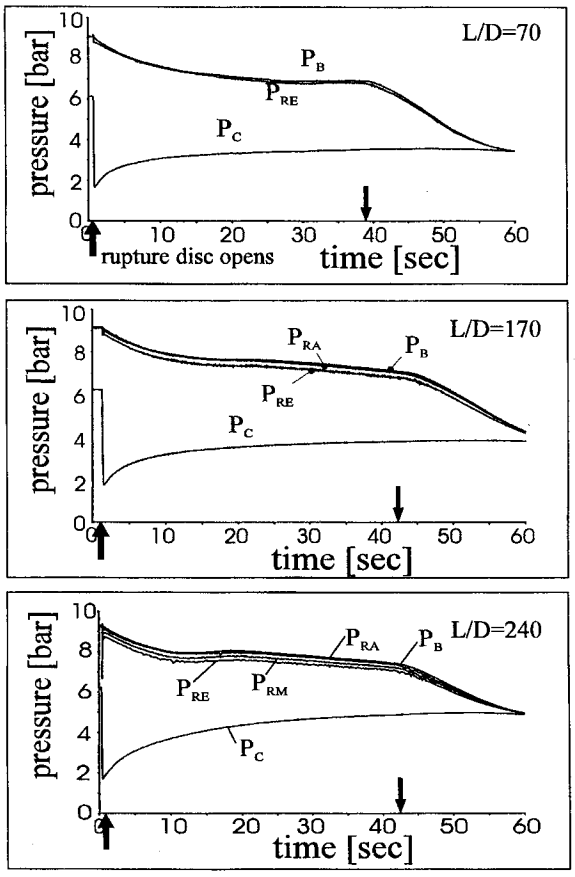

FIGURE 16 Pressure history (propane, orifice diameter $d_B = 5$ mm).

of the signals, given by the thermocouples in the various positions, as shown in Fig. 14, are presented versus the blow-down period. All thermocouples were emerged in liquid before the blow-down started. The lower diagram mediates the extent of thermodynamic non-equilibrium of the fluid in the vessel at any moment during the blow-down, by plotting the temperature readings versus the saturation line. The liquid remains superheated up to 6 K for a long time before the temperature suddenly drops. By comparing the liquid level with the thermocouple reading, one realizes that the temperature drops at that moment, when the liquid level falls below the thermocouple position. That means the liquid in the vessel mainly evaporates at its upper free surface and, as shown later, also immediately before entering the outlet nozzle at the bottom of the pipe. Inside the vessel, there is a large bulk of pure liquid, being superheated. This behavior is different from what was observed in the literature with depressurization from the top of the vessel, where flashing also starts near the upper surface of the liquid, however traveling down to the bottom of the vessel.

The length of the pipe, through which the flashing two-phase mixture flows is, of course, influencing the blow-down time, as shown in Fig. 16, presenting the pressure history for three different lengths with an orifice of 5 mm at the downstream end. The two arrows in this and the following figures indicate the moment when the burst disc opens (upward showing arrow), and when the liquid level in the pressure

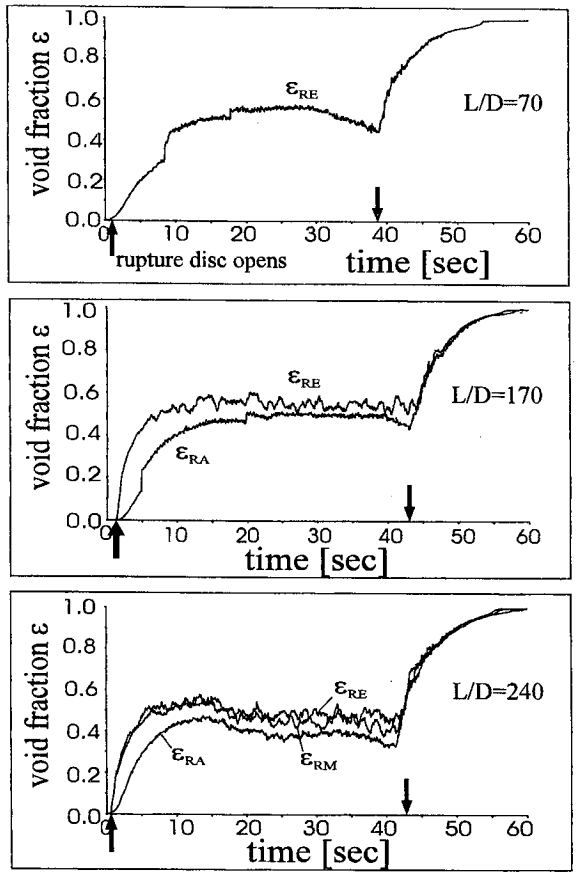

FIGURE 17 Void fraction history (propane, orifice diameter $d_B = 5$ mm).

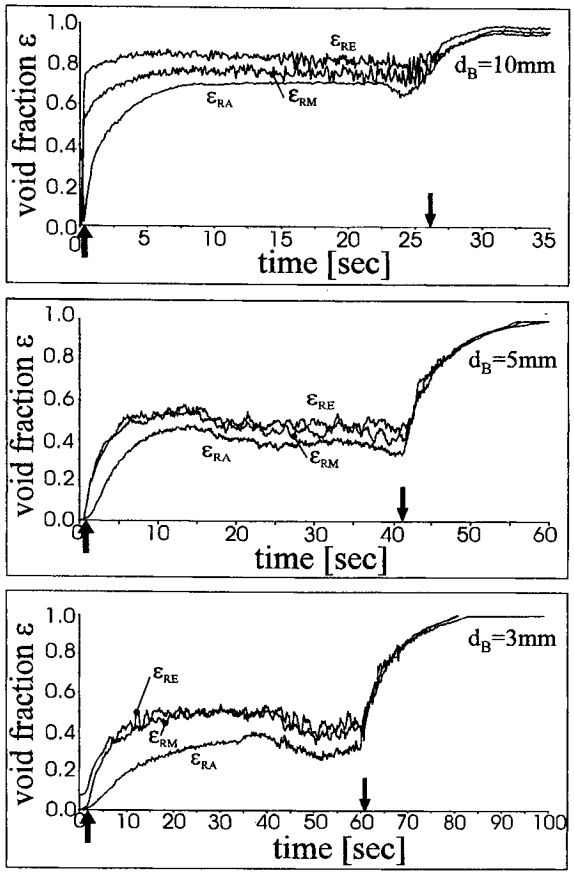

FIGURE 18 Time history of void fraction, influence of orifice diameter ($L/D = 240$, propane).

vessel falls below the position of the outstream nozzle.

The history of void fraction, presented in Fig. 17, is of greater interest. Immediately after the burst disc opens, the void fraction is growing rapidly and the largest amount of vapor is produced before or at the entrance to the tube. Along the tube, there is only a small increase in the void fraction. When the liquid level in the vessel falls below the outlet nozzle, the void fraction experiences another rise.

At the outlet- and the middle-position of the tube, oscillations in the void fraction can be observed. These oscillations originate from instabilities in the form of density-wave-oscillations, resulting from a highly complicated interaction between feeding fluid from the pressure vessel to the pipe and escaping flow out of the pipe through the orifice. The friction pressure drop in the pipe is a strong function of the void fraction, as is well known from the literature. So throttling in the orifice and two-phase friction in the pipe are in competition.

Of course, the throttling effect at the end of the pipe has a much stronger influence on the blow-down history than the length of the pipe, especially for $L/D > 50$. In Fig. 18, the void fraction history along a pipe of $L/D = 240$ is compared for three different orifice diameters. The strongest influence

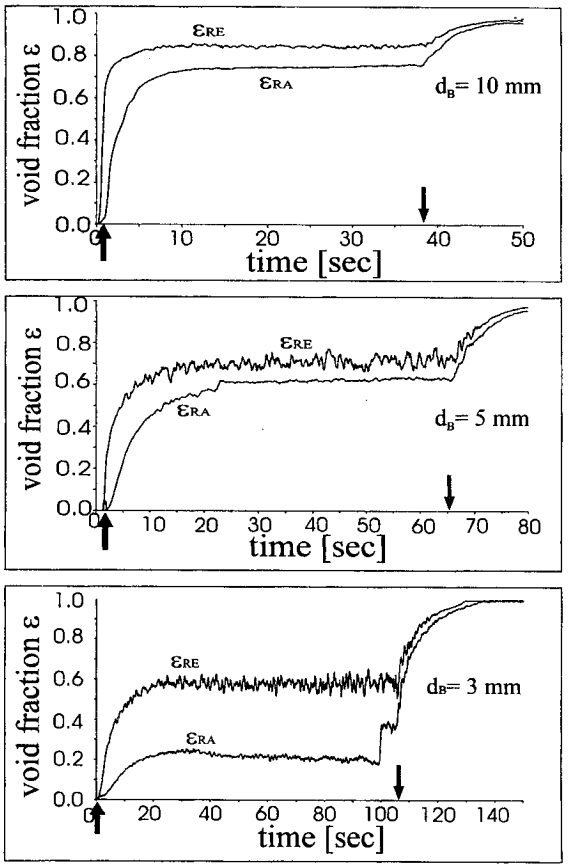

FIGURE 19 Time history of void fraction for binary mixture 50 percent propane and butane ($L/D = 240$).

of the orifice diameter can be observed at the upstream end of the tube. The void fraction there is much smaller at small orifice diameters than at larger ones, resulting in a stronger flashing along the tube.

This phenomenon becomes even more pronounced if we study a mixture of 50 mole percent of butane and propane. The lower diagram in Fig. 19 shows almost a doubling of the void fraction from the inlet to the outlet of the pipe, having a 3 mm orifice at its downstream end. The pipe in this case had an $L/D = 170$. Probably mixtures of highly volatile and low volatile components need a larger driving force for flashing than a fluid, consisting of one or the other pure component. In this connection, one certainly has to discuss the question how flashing occurs in a binary mixture. Is it a process of mass diffusion or are both components flashing equally with the higher volatile component, acting as nucleation sites? Further experiments, which try to monitor the concentration in the gas phase at any moment, should, perhaps, give an answer to this question. Figure 19 also mediates that the density oscillations at the downstream end of the pipe (position "RE") become stronger with decreasing orifice diameter.

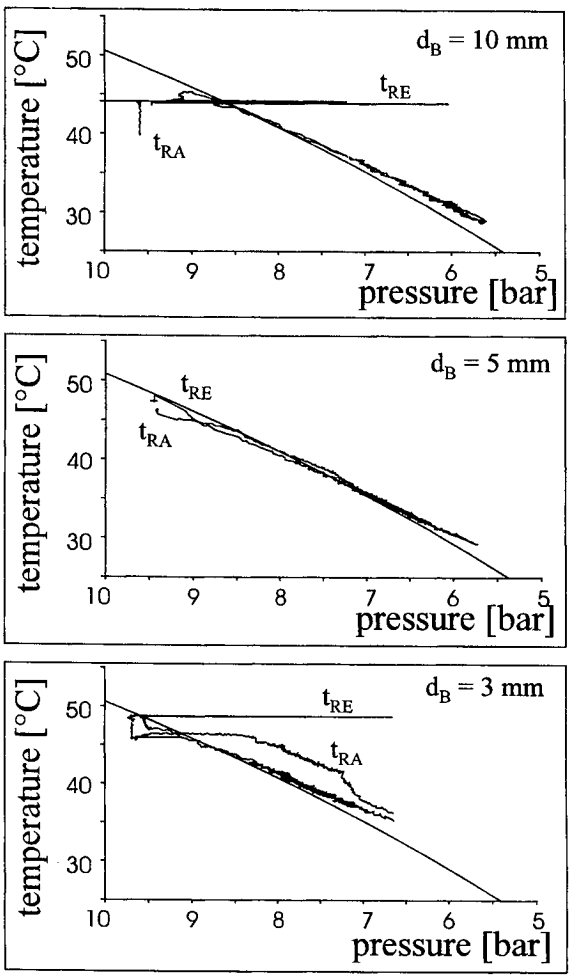

FIGURE 20 Thermodynamic non-equilibrium in the pipe with a 50 percent binary mixture of propane and butane.

The thermodynamic non-equilibrium in the pipe with the 50 percent mixture of butane and propane is demonstrated in Fig. 20, where the liquid temperature in the pipe is correlated with the saturation line. In correspondence with the behavior of the void fraction, discussed in Fig. 19, we observe a large superheating of the liquid — and, by this, a considerable thermodynamic non-equilibrium — at the upstream end (position "RA") of the pipe for the 3 mm orifice. With larger orifices, the temperature in the blow-down pipe follows the saturation line, which means that we have thermodynamic equilibrium. Only at the very first moment, we observe deviations from the saturation line, these are, however, due to the initial conditions in the pipe before starting the blow-down.

5. CONCLUDING REMARKS

Non-equilibria phenomena in two-phase flow—under transient conditions, as well as with steady flow—are still not well understood, even if modern measuring techniques, like holographic interferometry or capacitive sensors provide some insights into the physics of the flow. Mathematical modeling of two-phase flow made great progress in the last years, however, for a theoretically well-based description of the flow and a reliable prediction of flow effects, like pressure drop or void fraction during transients, we need much more quantitative information about thermodynamic, thermal and fluid-dynamic non-equilibria in boiling, and with blow-down. Young scientists should be encouraged to attack these problems with modern non-invasive and inertialess measuring techniques.

NOMENCLATURE

c	specific heat	kJ/kg K
c_p	specific heat at constant pressure	kJ/kg K
h	specific enthalpy	kJ/kg
h_{lg}	latent heat of evaporation	kJ/kg
Ja	Jacob number	—
$\dot{m}$	mass flow rate	kg/m^2 s
Nu	Nusselt number	—
p	pressure	bar
$\dot{q}$	heat flux density	kW/m^2
r	radial coordinate	m
Re	Reynolds number	—
t	time	s
T	temperature	K
z	axial coordinate	m

Greek Symbols

ε	void fraction	—
ϑ	temperature	0°C
ρ	density	kg/m^3

Subscripts

A	inlet
c	critical
C	containment
E	end
f	fluid
g	gas vapor
l	liquid
lg	liquid/gas
M	middle
s	saturated
v	vapor
0	wall

References

Bräuer, H., Stängl, G. and Mayinger, F. (1990) Onset of Nucleate Boiling with R12, *Proceedings of the 9th International Heat Transfer Conference*, Hemisphere, New York, Vol. 3, pp. 419–424.

Chen, Y.M., Nordmann, D. and Mayinger, F. (1991) Heat Transfer at the Phase Interface of Condensing Bubbles, In *Phase Interface Phenomena in Multiphase Flow*, Eds. G.F. Hewitt *et al.*, 1991. Hemisphere, New York, pp. 433–442.

Chen, Y.M. Wärmeübergang an der Phasengrenze kondensierender Blasen, Ph.D. Thesis, Technische Universität München, Germany, 1985.

Henry, R.E. and Fauske, H.K. (1971) The Two-Phase Critical Flow of One-Component Mixtures in Nozzles, Orifices and Short Tubes. Trans. ASME, *J. Heat Transfer*, **93**, 179.

Klug, F. and Mayinger, F. (1994) Impedance Based Flow Reconstruction—A Novel Flow Composition Measuring Technique for Multi-Phase-Flows, *Nuclear Engineering and Design*, **146**, 35–42.

Klug, F. and Mayinger, F. (1992) *Proceedings of NURETH-5 Meeting*, Salt Lake City, UT, Sept. 21–24.

Lautenschlager, G., Mayinger, F. and Wang, M.Y. (1994) Wetting of Dispersed Flow Film Boiling in Heated Bends, *Journal of Energy, Heat and Mass Transfer*, **16**, 35–45.

Mayinger, F. and Panknin, W. (1974) Holography in Heat and Mass Transfer, *Proceedings of the 5th International Heat Transfer Conference*, Vol. VI, pp. 28–43.

Mayinger, F. (1994). Optical Measurements, Techniques and Applications, Springer Verlag, Heidelberg.

Mayinger, F. and Wang, M.Y. (1994). On the Mechanism of Dispersed Flow Heat Transfer in the Circular Bend, *Proceedings of the 10th International Heat Transfer Conference*, Brighton, UK, Vol. FB 17, pp. 503–508.

Mayinger, F., Tong, K. and Wallner, J. (1995) Flashing Void Fraction and Pressure Drop in Pipes During Rapid Depressurisation, *ANS Proceedings, National Heat Transfer Conference*, Portland, Oregon, USA, HTC, Vol. 8, pp. 237–246.

Mersmann, A. (1977) Auslegung und Maßstabsvergrößerung von Blasen und Tropfensäulen. *Chem.-Ing.-Tech.*, **49**, 679–770.

Moody, F.J. (1965) Maximum Flow Rate of a Single Component, Two-Phase Mixture, *J. Heat Transfer, Trans. ASME*, **87**, 134.

Nordmann, D. and Mayinger, F. (1981) Temperatur, Druck und Wärmetransport in der Umgebung kondensierender Blasen, *VDI-Forschungsheft*, 605.

Sozzi, G.L. and Sutherland, W.A. (1975) Critical Flow of Saturated and Subcooled Water at High Pressure. *ASME Non-Equilibrium Two-Phase Flows Symp.* (Ref. [1]), pp. 19–26.

Sterman, L.S. (1965) The Correlation of Experimental Data for Vapour Bubbling Through a Liquid. *Zh. Tech. Fiz*, **26**, 1519.

Viecenz, H.-J. (1980) Blasenaufstieg und Phasenseparation in Behältern bei Dampfeinleitung und Druckentlastung, Dissertation, Technische Universität Hannover, Hannover, Germany.

Wang, M.Y. (1993) Phasenverteilung, Sekundärströmung und Wärmeübergang bei Sprühkühlung in Krümmern, Ph.D. Thesis, Technische Universität München, Munich, Germany.